

Mott-Hubbard versus charge-transfer behavior in LaSrMnO₄ studied via optical conductivity

A. Gössling, M. W. Haverkort, M. Benomar, Hua Wu, D. Senff, T. Möller, M. Braden, J. A. Mydosh, and M. Grüninger
II. Physikalisches Institut, Universität zu Köln, Zùlpicher Str. 77, 50937 Köln, Germany
 (Received 21 September 2007; published 8 January 2008)

Using spectroscopic ellipsometry, we study the optical conductivity $\sigma(\omega)$ of insulating LaSrMnO₄ in the energy range of 0.75–5.8 eV from 15 to 330 K. The layered structure gives rise to a pronounced anisotropy. A multipeak structure is observed in $\sigma_1^a(\omega)$ ($\sim 2, 3.5, 4.5, 4.9,$ and 5.5 eV), while only one peak is present at 5.6 eV in $\sigma_1^c(\omega)$. We employ a local multiplet calculation and obtain (i) an excellent description of the optical data, (ii) a detailed peak assignment in terms of the multiplet splitting of Mott-Hubbard and charge-transfer absorption bands, and (iii) *effective* parameters of the electronic structure, e.g., the on-site Coulomb repulsion $U_{\text{eff}}=2.2$ eV, the in-plane charge-transfer energy $\Delta_d=4.5$ eV, and the crystal-field parameters for the d^4 configuration ($10Dq=1.2$ eV, $\Delta_{eg}=1.4$ eV, and $\Delta_{t2g}=0.2$ eV). The spectral weight of the lowest absorption feature (at 1–2 eV) changes by a factor of 2 as a function of temperature, which can be attributed to the change of the nearest-neighbor spin-spin correlation function across the Néel temperature $T_N=133$ K. Interpreting LaSrMnO₄ effectively as a Mott-Hubbard insulator naturally explains this strong temperature dependence, the relative weight of the different absorption peaks, and the pronounced anisotropy. By means of transmittance measurements, we determine the onset of the optical gap $\Delta_{\text{opt}}^a=0.4\text{--}0.45$ eV at 15 K and $0.1\text{--}0.2$ eV at 300 K. Our data show that the crystal-field splitting is too large to explain the anomalous temperature dependence of the c -axis lattice parameter by thermal occupation of excited crystal-field levels. Alternatively, we propose that a thermal population of the upper Hubbard band gives rise to the shrinkage of the c -axis lattice parameter.

DOI: [10.1103/PhysRevB.77.035109](https://doi.org/10.1103/PhysRevB.77.035109)

PACS number(s): 71.20.Be, 71.27.+a, 75.47.Lx, 78.20.–e

I. INTRODUCTION

The insulating behavior of many transition-metal (TM) compounds with a partially filled $3d$ shell is a clear manifestation of strong electronic correlations. In the Zaanen-Sawatzky-Allen scheme,¹ these correlated insulators are categorized into Mott-Hubbard (MH) and charge-transfer (CT) types. In the former, the on-site Coulomb repulsion U is larger than the bandwidth W ; thus, the conduction band splits into lower and upper Hubbard bands (LHB and UHB) (see Fig. 1). At half filling, the lowest electronic excitation is from LHB to UHB, $d^n d^n \rightarrow d^{n-1} d^{n+1}$, where d^n denotes a TM ion with n electrons in the $3d$ shell. In a CT insulator, U is larger than the charge-transfer energy Δ ; thus, the LHB is pushed below the highest occupied band of the ligands, e.g., O $2p$ (see Fig. 1). Here, the lowest electronic excitation is from O $2p$ to UHB, $p^6 d^n \rightarrow p^5 d^{n+1}$. Typically, early TM compounds are of MH type, whereas late ones such as the high- T_c cuprates belong to the CT class.²

For manganites with $\text{Mn}^{3+} 3d^4$ configuration, e.g., LaMnO₃ or LaSrMnO₄, the characterization is not as straightforward. The analysis of photoemission data indicates $U \gtrsim \Delta$, i.e., a CT character.³ Yet, most theoretical approaches employ an effective Hubbard model (see below). Both MH and CT types have been proposed on the basis of optical data.^{2,4–10} For $U \gg \Delta$ or $U \ll \Delta$, there are different ways to disentangle MH and CT excitations in the optical conductivity. First, the spectral weight of CT excitations is larger, e.g., $\sigma_1(\omega) \sim 500$ ($\Omega \text{ cm}$)⁻¹ for MH and ~ 5000 ($\Omega \text{ cm}$)⁻¹ for CT excitations in LaTiO₃.² This can be attributed to the $\text{TM}_{3d}\text{-O}_{2p}$ hopping amplitude t_{pd} : $\sigma_1(\omega) \propto t_{pd}^2$ for CT and $\propto t_{pd}^4/\Delta^2$ for MH excitations (see below). Second, the polarization dependence may be very different, depending on the crystal structure. In layered LaSrMnO₄, the interlayer

Mn-Mn hopping is strongly suppressed; thus, the contribution of MH excitations should be negligible in $\sigma_1^c(\omega)$. In contrast, CT excitations contribute to both $\sigma_1^a(\omega)$ and $\sigma_1^c(\omega)$ due to the octahedral O coordination of the Mn sites. Third, the spin and orbital selection rules are different, giving rise to a different behavior of the spectral weight as a function of temperature T .^{8–18} As an example, we consider a MH insulator with a single $3d$ band and one electron per TM site. In the case of ferromagnetic order, the spectral weight of MH excitations is zero due to the Pauli principle (neglecting spin-orbit coupling, the total spin is conserved in an optical exci-

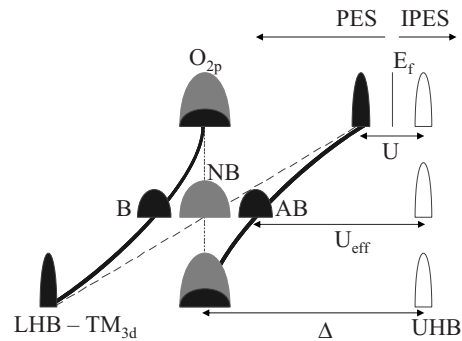


FIG. 1. Sketch of the density of states [photoemission (PES) and inverse photoemission (IPES) spectra] for a single, half-filled $3d$ orbital and degenerate, full O $2p$ orbitals. The on-site Coulomb repulsion U increases from top to bottom, whereas the charge-transfer energy Δ is assumed to be constant. E_f denotes the Fermi level. Top: Mott-Hubbard insulator for $U \ll \Delta$. Bottom: charge-transfer insulator for $U \gg \Delta$. In the absence of hybridization, the bands follow the straight lines with increasing U . With hybridization, one has to distinguish bonding (B), antibonding (AB, both black), and non-bonding bands (NB, gray).

tation). Thus, one expects a drastic change of the spectral weight upon heating across the magnetic ordering temperature. In contrast, the O $2p$ band is completely filled and the spectral weight of CT excitations is independent of the magnetic properties. For comparison with experimental data, the orbital multiplicity has to be taken into account and the optical spectra of MH excitations contain valuable information on orbital occupation and nearest-neighbor spin and orbital correlations. This kind of analysis has been applied to a number of different TM compounds (Mn, V, Ru, Mo).^{8–18} In LaMnO_3 , there is some disagreement on the experimental side: LaMnO_3 has been interpreted as MH type due to a pronounced T dependence observed by spectroscopic ellipsometry⁹ and as CT type due to the absence of a significant T dependence across the Néel temperature T_N in reflectivity measurements.⁸ Note that it is still unclear in which compounds this kind of analysis can be applied. For instance, in YTiO_3 , the lowest MH excitation shows a strong T dependence but only a weak dependence on the magnetic properties.¹⁹ However, our analysis of LaSrMnO_4 fully corroborates the intimate relation between spectral weight and magnetism reported by Kovaleva *et al.*⁹ for LaMnO_3 .

Does this prove that LaMnO_3 and LaSrMnO_4 are of MH type? The d^5 configuration is particularly stable. Thus, the d^4 configuration has a strong $d^5\bar{L}$ contribution, where \bar{L} denotes a ligand hole and the O $2p$ orbitals certainly play an important role. As stated above, with $U \geq \Delta$,³ the manganites may be categorized as CT type. However, for the analysis of, e.g., optical data, it is important to consider the symmetry. Let us discuss the simplified case of a single, half-filled $3d$ band and degenerate, full O $2p$ bands. Due to hybridization, one has to distinguish bonding (B), antibonding (AB), and non-bonding (NB) bands below the Fermi level (see Fig. 1). The AB band is the highest occupied one. It has mainly TM character for $U \ll \Delta$ and mainly O character for $U \gg \Delta$. For the intermediate situation $U \sim \Delta$, the character is strongly mixed. However, in the manganites with a less than half-filled $3d$ shell, the *symmetry* of the AB band is determined by the symmetry of the $3d$ band, i.e., it can be described in terms of a Wannier orbital with d symmetry centered around a Mn site. In particular, the spin and orbital selection rules mentioned above for a MH insulator apply also to the AB band. These selection rules are most important for understanding the optical data. For instance, in LaSrMnO_4 , one expects that the AB band shows the pronounced anisotropy and the strong temperature dependence discussed above for the MH case. Thus, “MH or CT” is not the essential question for $U \sim \Delta$ and strong hybridization. In this sense, we analyze our data in terms of an *effective* Hubbard model with a rather small value of $U_{\text{eff}} = 2.2$ eV. Excitations from NB to UHB are treated as CT and from AB to UHB as MH. We find that these effective MH excitations are significantly lower than the CT excitations. The effective model does not contain the B band, which is important for optical or photoemission measurements at higher energies. However, we fully take into account the multiplet splitting of the MH and CT bands caused by the multiorbital structure of the $3d$ shell.

Here, we focus on LaSrMnO_4 , which crystallizes in the layered K_2NiF_4 structure with tetragonal symmetry $I4/mmm$.²⁰ The lattice constants at room temperature are a

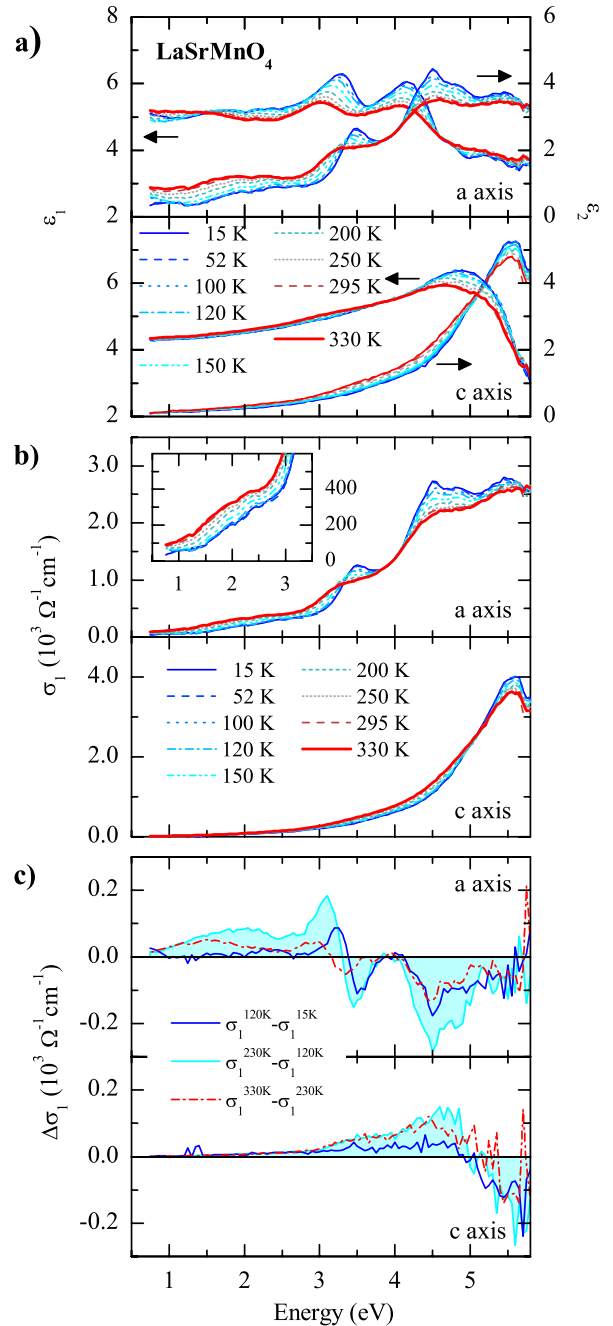


FIG. 2. (Color online) [(a) and (b)] Dielectric constant and optical conductivity of LaSrMnO_4 for the a and c directions between 0.75 and 5.80 eV for different temperatures. (c) Change of the optical conductivity: $\sigma_1(330 \text{ K}) - \sigma_1(230 \text{ K})$, $\sigma_1(230 \text{ K}) - \sigma_1(120 \text{ K})$, and $\sigma_1(120 \text{ K}) - \sigma_1(15 \text{ K})$.

$= 3.786 \text{ \AA}$ and $c = 13.163 \text{ \AA}$. All Mn ions have a nominal valence of +3 ($3d^4$ with spin $S=2$). Antiferromagnetic order has been observed below $T_N = 133 \text{ K}$.^{21–23} Neglecting hybridization, the four $3d$ electrons occupy the xy , yz , zx , and $3z^2 - r^2$ orbitals with parallel spins, while $x^2 - y^2$ is empty.²⁴ Similar to LaMnO_3 , also the character of LaSrMnO_4 — MH vs CT — has been discussed controversially.^{4,7,25–29} Previous optical studies reported $\sigma_1^a(\omega)$ for 300 K (Ref. 4) and very recently for 10 K.⁷ By means of spectroscopic ellipsometry,

we determine the optical-conductivity tensor $\sigma(\omega)$ between 0.75 and 5.8 eV as a function of temperature. Using a local multiplet calculation, we interpret the observed absorption bands in terms of effective Mott-Hubbard and charge-transfer excitations. This assignment utilizes the points raised above, i.e., the pronounced anisotropy, the difference in spectral weight, and the strong temperature dependence of the spectral weight. Using transmittance measurements, we determine the optical gap $\Delta_a=0.4\text{--}0.45$ eV at 15 K and 0.1–0.2 eV at 300 K. Our data indicate that the anomalous shrinkage of the c -axis lattice parameter with increasing temperature cannot be attributed to a thermal occupation of *local* crystal-field levels^{22,30,31} but rather to a thermal population of the UHB.

Section II describes the experimental details. Our optical data and a detailed analysis of the spectral weight are reported in Sec. III. The local multiplet calculation, the effective parameters of the electronic structure, and the calculation of $\sigma(\omega)$ based on the multiplet calculation are discussed in Sec. IV. Finally, in Sec. V, we discuss the peak assignment in terms of the multiplet splitting of MH and CT absorption bands, the relationship between the spectral weight and superexchange, and the anomalous thermal expansion.

II. EXPERIMENT

Single crystals of LaSrMnO₄ have been grown using the floating zone technique following Ref. 20. The sample quality and stoichiometry were checked using polarization mi-

croscopy, neutron diffraction, and x-ray diffraction. The two nonvanishing, complex entries ϵ^a and ϵ^c of the dielectric tensor for tetragonal symmetry were determined using a rotating-analyzer ellipsometer (Woollam VASE) equipped with a retarder between polarizer and sample. By measuring on a polished ac surface, we determined the normalized Müller matrix elements $m_{ij}^k=M_{ij}^k/M_{11}^k$ ($i=1\text{--}3$, $j=1\text{--}4$, $k=1\text{--}2$),³² where $k=1$ (2) corresponds to measurements with the a (c) axis perpendicular to the plane of incidence. The

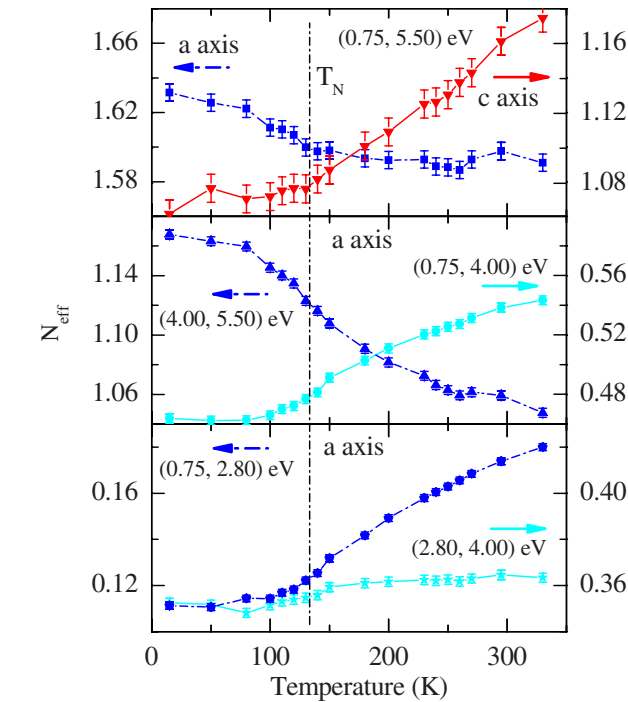


FIG. 3. (Color online) Top: effective carrier concentration $N_{\text{eff}}(\omega_1, \omega_2)$ for the a and c directions with $\omega_1=0.75$ eV and $\omega_2=5.5$ eV. Middle and bottom: N_{eff} for the a direction for different energy ranges.

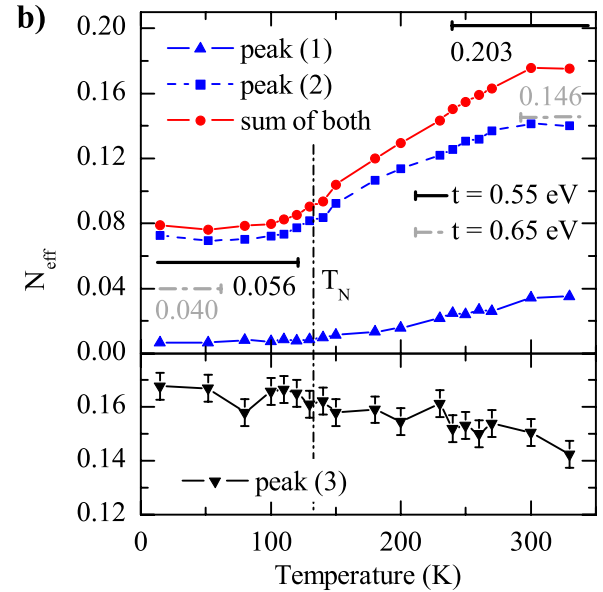
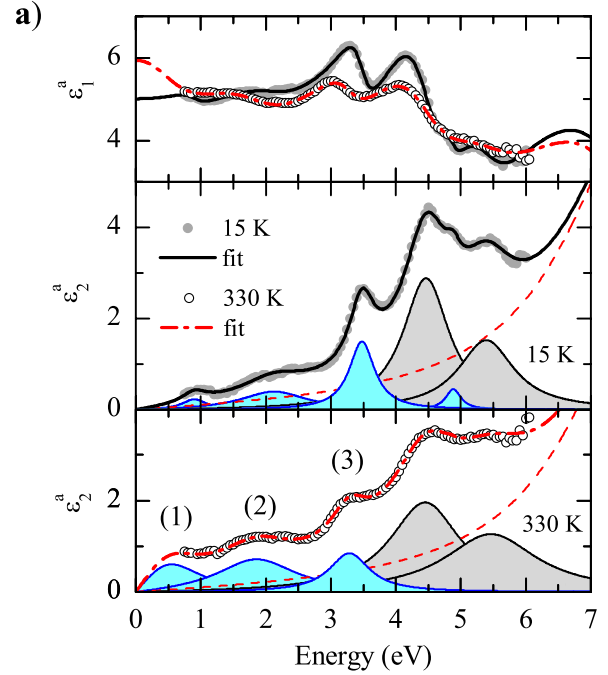


FIG. 4. (Color online) (a) Lorentzian fit of ϵ_1^a (top panel) and ϵ_2^a (middle and bottom) for $T=15$ and 330 K. (b) N_{eff} of peaks (1)–(3) as obtained from the Drude-Lorentz fit. The horizontal lines indicate theoretical estimates of N_{eff} for $T \ll T_N$ and $T \gg T_N$ as derived from the kinetic energy for an effective Mn-Mn hopping amplitude $t=0.55\text{--}0.65$ eV (see Sec. V C).

angle of incidence was 70° . We obtained ε^a and ε^c by fitting the nonvanishing elements m_{12}^k , m_{21}^k , m_{33}^k , and m_{34}^k .³³ We have checked that the results fulfill the Kramers-Kronig consistency. The ellipsometric measurements have been performed from 15 to 330 K in a UHV cryostat with $p < 10^{-9}$ mbar. The effect of the cryostat windows has been determined using a standard Si wafer. Our data are consistent with spectra of Refs. 4 and 7.

In order to determine the optical gap, we measured the transmittance from 5 to 300 K using a Fourier-transform spectrometer (Bruker IFS 66v). The sample was approximately $70 \mu\text{m}$ thick and has been prepared in the same way as described above.

III. RESULTS

A. Ellipsometry and interband excitations

In Fig. 2(a), we plot $\varepsilon^l = \varepsilon_1^l + i\varepsilon_2^l$ ($l=a, c$) from 0.75 to 5.8 eV. For convenience, the real part $\sigma_1 = (\omega/4\pi) \varepsilon_2$ of the optical conductivity is displayed in Fig. 2(b). We find a striking anisotropy. In particular, there is only one strong peak at 5.6 eV in σ_1^c , while a multipeak structure is present in σ_1^a (peaks at $\sim 2, 3.5, 4.5, 4.9,$ and 5.5 eV). All peaks show a strong temperature dependence. With increasing T , σ_1^a increases below ~ 3 eV and decreases above ~ 4 eV. In particular, spectral weight (SW) is transferred from 3.5 to 3.0 eV and from 4.5 to 2.0 eV [see Fig. 2(c)].

We analyze the T dependence of the SW using the effective carrier concentration N_{eff} ,

$$N_{\text{eff}}(\omega_1, \omega_2) = \frac{2mV}{\pi e^2} \int_{\omega_1}^{\omega_2} \sigma_1(\omega) d\omega, \quad (1)$$

where m denotes the electron mass, V the unit cell volume, and e the electron charge. Equation (1) translates into the f -sum rule for $\omega_1 \rightarrow 0$ and $\omega_2 \rightarrow \infty$.³⁴ As shown in Fig. 3, the total spectral weight $N_{\text{eff}}(0.75\text{eV}, 5.5\text{eV})$ decreases (increases) with increasing T for the a (c) direction. In σ_1^a , we find an isosbestic point at $\omega_i \approx 4.0$ eV. The corresponding transfer of SW is evident from the comparison of $N_{\text{eff}}(0.75\text{eV}, 4.0\text{eV})$ and $N_{\text{eff}}(4.0\text{eV}, 5.5\text{eV})$ (see middle panel of Fig. 3). The transfer of SW sets in roughly 30 K

below $T_N = 133$ K, but the curves possess an inflection point approximately at T_N .

The direct integration of $\sigma_1(\omega)$ in Eq. (1) has the advantage to be model independent. For a more detailed analysis of the T dependence of the individual absorption bands, we fit ε_1 and ε_2 simultaneously using a sum of Drude-Lorentz oscillators,³⁴

$$\varepsilon(\omega) = \varepsilon_\infty + \sum_j \frac{\omega_{p,j}^2}{\omega_{0,j}^2 - \omega^2 - i\gamma_j\omega}, \quad (2)$$

where $\omega_{0,j}$, $\omega_{p,j}$, and γ_j are the peak frequency, the plasma frequency, and the damping of the j th oscillator, and ε_∞ denotes the dielectric constant at “infinite” frequency (i.e., above the measured region). The plasma frequency is related to the spectral weight of a single Lorentzian,³⁴ $\int_0^\infty \sigma_1(\omega) d\omega = \omega_p^2/8$.

Using seven oscillators, we obtain an excellent description of both ε_1^a and ε_2^a , which clearly demonstrates the Kramers-Kronig consistency [see Fig. 4(a)]. The peak frequency of one of these seven oscillators is outside the measured region (dashed line). It corresponds to the strong feature observed at about 7 eV by Moritomo *et al.* at room temperature.⁴ The parameters ω_0 and γ of this strong oscillator have been assumed to be independent of T . Since ellipsometry determines both ε_1 and ε_2 independently, the contributions of higher-lying bands to the measured region can be fixed quite accurately. For the lowest three oscillators, the effective carrier concentration N_{eff} obtained from the fit is displayed in Fig. 4(b). With increasing T , the SW of peak (3) at 3.5 eV decreases by $\sim 20\%$, while the SW of peaks (1) and (2) at 1–2 eV increases by a factor of 2. Comparing the T dependence of N_{eff} below about 3 eV as obtained either from the Drude-Lorentz fit [Fig. 4(b)] or from the direct integration of $\sigma_1(\omega)$ (bottom panel of Fig. 3), the former is even stronger because it separates contributions from higher-lying bands. The precise determination of N_{eff} is important for the comparison with the kinetic energy (see Sec. V C below).

We find the same trend in the c direction. The change of the SW of $\sim 10\%$ obtained from direct integration of $\sigma_1^c(\omega)$ may be influenced by a broadening or shift of the peak (since

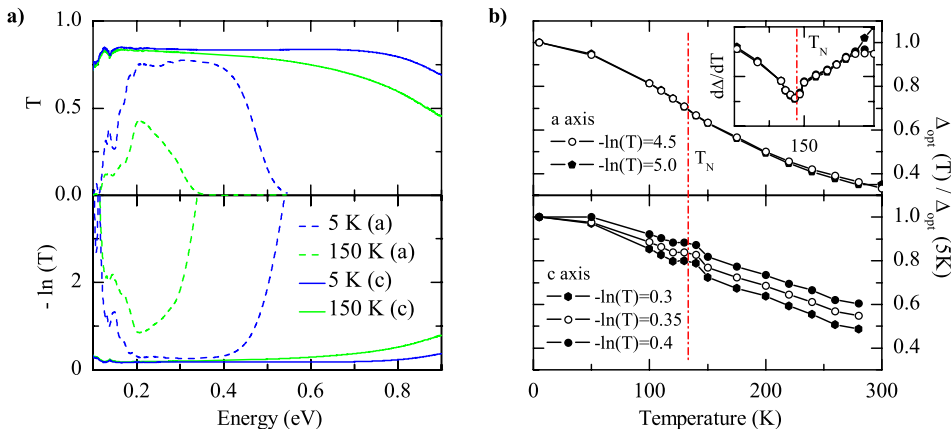


FIG. 5. (Color online) (a) Transmittance T (top panel) of a thin LaSrMnO_4 sample ($d \sim 70 \mu\text{m}$) and $-\ln(T) \propto \alpha$ for 5 and 150 K. (b) Evolution of the onset of the optical gap as determined from $-\ln(T) = \text{const.}$

TABLE I. Effective electronic parameters obtained from the multiplet calculation by fitting the optical data for $T=15$ K. The factor r is dimensionless; all other units are in eV.

F^0	r	$10Dq(d^4)$	$\Delta_{t_{2g}}(d^4)$	$\Delta_{e_g}(d^4)$	Δ_a	Δ_c
1.20	0.64	1.20	0.2	1.4	4.51	4.13

it is close to the edge of the measured frequency range) or by a change in the background originating from higher-lying bands. In a fit based on Eq. (2), we found a larger change in SW of $\sim 20\%$.

B. Transmittance and gap

Figure 5(a) shows the transmittance T and $-\ln(T) \propto \alpha(\omega)$ from 0.1 to 0.9 eV for both a and c polarizations. Here, $\alpha(\omega)$ denotes the absorption coefficient. The calculation of $\sigma_1(\omega)$ additionally requires the knowledge of the reflectivity R in this frequency range. The transmittance is a very sensitive probe in order to determine the onset Δ_{opt} of the optical gap. For this purpose, α and σ_1 can be used equivalently. Assuming a reasonable value of $R=0.15-0.2$, we find $\sigma_1^a \sim 1(\Omega \text{ cm})^{-1}$ at 0.5 eV at 5 K, more than 2 orders of magnitude smaller than at 2 eV. Thus, the data in Fig. 5 only show the very onset of excitations across the gap. The absorption below about 0.2 eV can be attributed to weak (multi)phonon excitations.

From linear extrapolation of $-\ln(T)$ to zero, we find $\Delta_{\text{opt}}^a = 0.40-0.45$ eV and $\Delta_{\text{opt}}^c > 0.9$ eV at 5 K. In order to monitor the temperature dependence of the onset of the gap, we solve the equations $-\ln(T^a) = m_a$ and $-\ln(T^c) = m_c$ with $m_a = 5.0$ and 4.5 and $m_c = 0.40, 0.35$, and 0.30, respectively, where a and c denote the polarization direction. The results are shown in Fig. 5(b). At 300 K, we find $\Delta_{\text{opt}}^a = 0.1-0.2$ eV. The redshift of the onset of the gap with increasing T can be attributed to either a shift of the peak frequency or an increase of the bandwidth. According to the fit results, peak (1) shifts by about 0.3 eV from 5 to 300 K [see Fig. 4(a)]. This shift may originate from thermal expansion and electron-phonon coupling,^{35,36} giving rise to a change of the effective crystal field. The bandwidth W may change due to either a change of

the lattice parameters or of the spin-spin correlations (W is reduced in the antiferromagnetically ordered state). The plot of the derivative $d\Delta_{\text{opt}}^a/dT$ in the inset of Fig. 5(b) and the lower panel clearly show that $\Delta_{\text{opt}}(T)$ changes its slope at $T_N=133$ K (independent of the choice of m_a and m_c), which reflects the behavior of the lattice constants.²²

IV. MULTIPLET CALCULATION

One may expect that a local multiplet calculation for a single 180° Mn-O-Mn bond yields a reasonable assignment of the CT ($d^4p^6 \rightarrow d^5p^5$) and MH excitations ($d^4d^4 \rightarrow d^3d^5$) of the undoped Mott insulator LaSrMnO₄. For simplicity, we neglect hybridization; thus, the two-site states are a simple product of two single-site states. This affects the excitation energies and the matrix elements. Thus, we obtain renormalized parameters, e.g., an effective value of U_{eff} , which has to be kept in mind for comparison with results from other techniques. The selection rules are not affected by hybridization, as stated in the Introduction. We calculated $\sigma_1^a(\omega)$ and $\sigma_1^c(\omega)$ by evaluating the matrix elements between all multiplet states. For more details, we refer to the Appendix and Ref. 33.

The multiplet calculation takes into account the Coulomb interaction and the crystal-field splitting. The former is described by the Slater integrals F^0 , F^2 , and F^4 .^{37,38} We use only two parameters, F^0 and the reduction factor r in $F^k(d^n) = rF_{\text{HF}}^k(d^n)$ for $k=2$ and 4, where $F_{\text{HF}}^k(d^n)$ denotes Hartree-Fock results for a free d^n ion. For the d^n states, the tetragonal crystal field is parametrized by $10Dq$, $\Delta_{t_{2g}}$, and Δ_{e_g} , representing the splitting between t_{2g} and e_g levels and the splitting within these levels, respectively. The CT energy is given by $\Delta_l = E_0(d^5) + E(p^5) - E_0(d^4) - E(p^6)$ for $l=a$ or c , where $E_0(d^n)$ is the lowest energy of the d^n multiplets. The p^5 states are assumed to be degenerate. These seven electronic parameters (see Table I) determine all peak frequencies and the relative weight of different peaks within one polarization. A constrained fit of the experimental data requires seven more parameters (for the width, the absolute value, and higher-lying bands, see the Appendix). Altogether, we use 14 parameters, i.e., much less than those in the Drude-Lorentz model (22 parameters only for the a direc-

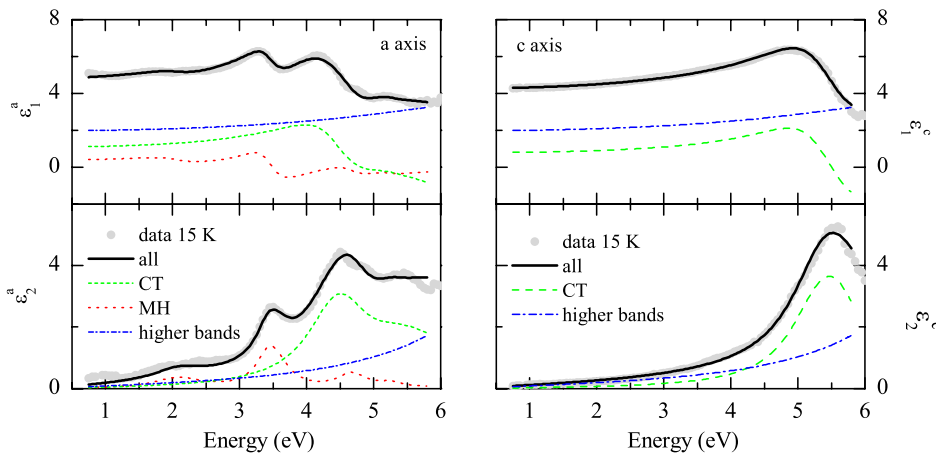


FIG. 6. (Color online) Comparison between ϵ as obtained from the multiplet calculation and the measured data at 15 K.

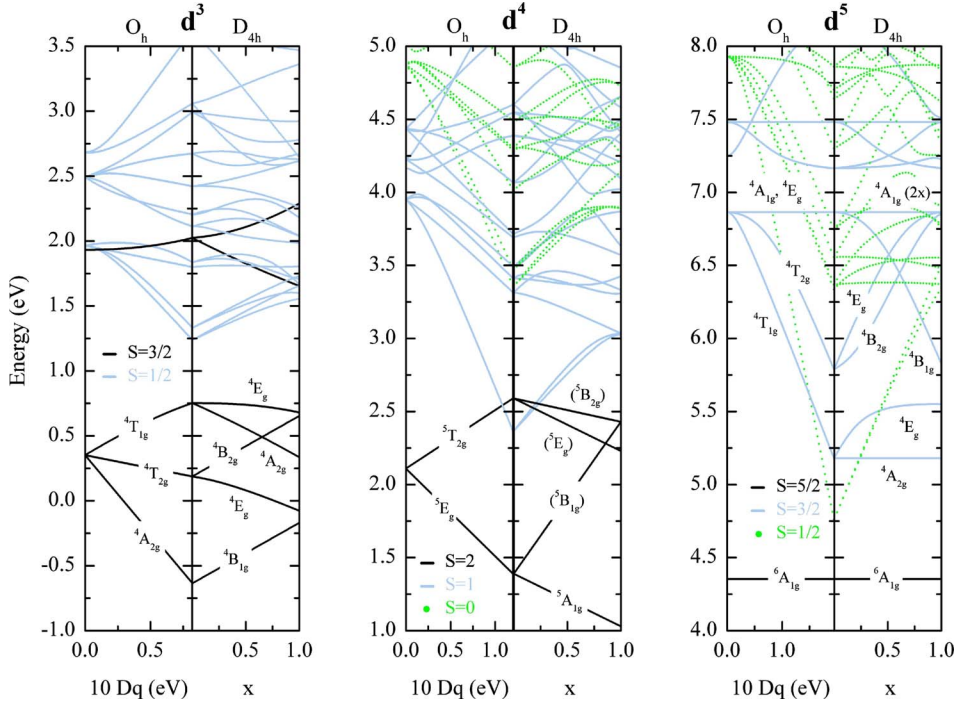


FIG. 7. (Color online) Energy level diagrams from the multiplet calculation for the d^3 , d^4 , and d^5 configurations as a function of $10Dq$ in O_h and as a function of x in D_{4h} for a fixed value of $10Dq$. The control parameter x denotes the strength of Δ_{eg} and Δ_{t2g} ; $x=1$ represents the full strength used for the spectra shown in Fig. 6. The low-lying multiplets are labeled by their irreducible representations in D_{4h} ; those being not relevant for the optical transitions are shown in brackets. The electronic fit parameters can be found in Ref. 33 and are summarized in Table I (for more details, see the Appendix and Ref. 33).

tion, see above). Moreover, the discussion of the peak assignment below will show that the pronounced structure of the experimental spectra provides severe constraints for the electronic parameters. The spectra with the lowest χ^2 are plotted in Fig. 6. The overall agreement is excellent. We find $F^0=1.2$ eV and $r=0.64$, resulting in $U_{\text{eff}}=2.2$ eV and Hund's coupling $J_H=0.6$ eV (cf. Ref. 39). The energy levels of the d^3 , d^4 , and d^5 multiplets are shown in Fig. 7 as a function of the crystal-field parameters.

V. DISCUSSION

Our first goal is to disentangle CT excitations $d^4p^6 \rightarrow d^5p^5$ and MH excitations $d^4d^4 \rightarrow d^3d^5$. As discussed in the Introduction, the spectral weight of MH excitations is weaker. In layered LaSrMnO_4 , the interlayer Mn-Mn hopping is strongly suppressed and MH excitations can be neglected in the c direction. This is the main reason for the pronounced anisotropy observed experimentally and suggests the following interpretation: the peak at ~ 5.6 eV in $\varepsilon_2^c(\omega)$ is a CT excitation and the same holds true for the strong excitations in the same energy range in $\varepsilon_2^a(\omega)$. The weaker features below ~ 4 eV in $\varepsilon_2^a(\omega)$ are MH excitations. The detailed analysis discussed below will support this assignment.

A. Charge-transfer excitations

In the c direction, we attribute the whole spectral weight to a CT peak at 5.6 eV and to the onset of higher-lying processes. To get an idea about the initial and final states of this CT excitation, we start from the strong crystal-field limit (i.e., neglect electron-electron interactions). In the d^4 ground state, the tetragonally distorted MnO_6 octahedra indicate that three electrons occupy the xy , yz , and zx orbitals and the

fourth electron occupies the $d_{3z^2-r^2}$ orbital,^{22,24} whereas $d_{x^2-y^2}$ remains unoccupied (see Fig. 8). This is supported by our multiplet calculation. In the initial state d^4p^6 , all O 2p orbitals are occupied; thus, the excitation and its selection rules are dominated by the d^5 part of the final state d^5p^5 . According to the spin selection rule, only d^5 states with $S=5/2$ or $3/2$ can be reached from the d^4 $S=2$ ground state. Following Hund's rule, the lowest d^5 state corresponds to a high-spin $S=5/2$ multiplet, in which the five 3d orbitals are equally occupied. For the orbital selection rules, one thus has to consider the overlap between the O 2p orbitals and the initially unoccupied $d_{x^2-y^2}$ orbital. This is only finite along the a direction but zero along c . Therefore, we cannot identify the peak at 5.6 eV in ε_2^c with the lowest CT transition. The second lowest CT excitation in the strong crystal-field limit corresponds to a transfer of one electron from O 2p into the degenerate d_{xz}/d_{yz} orbitals, i.e., to a final state with $3d^5$ $S=3/2$. The overlap is finite, both in the a and c directions. This assignment of the peak at 5.6 eV in ε_2^c is sup-

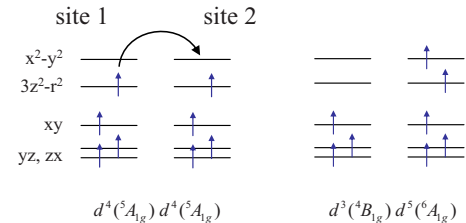


FIG. 8. (Color online) Sketch of the lowest Mott-Hubbard excitation in LaSrMnO_4 in the strong crystal-field limit, i.e., configuration mixing is neglected. In the final state, the d^5 site is in a high-spin $S=5/2$ configuration. This excitation is assigned to the feature observed around 2 eV in $\sigma_1^a(\omega)$. The spectral weight is largest for parallel alignment of neighboring spins.

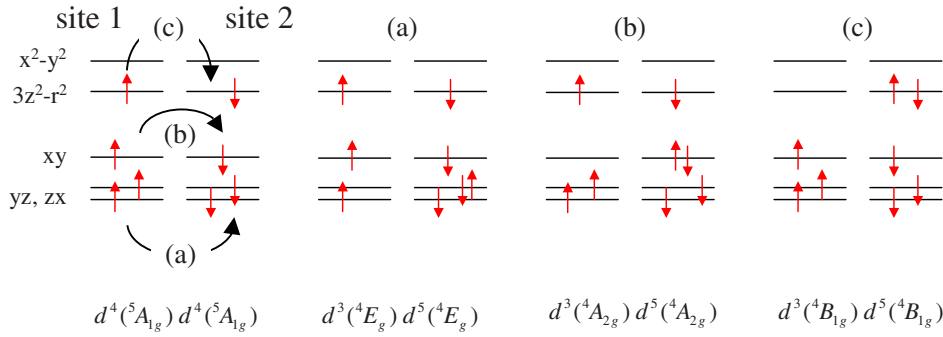


FIG. 9. (Color online) Sketch of Mott-Hubbard excitations to final states with $S(d^5)=3/2$. These excitations are degenerate in the strong crystal-field limit and are assigned to the peak at 3.5 eV in $\sigma_1^a(\omega)$. The spectral weight is largest for an antiferromagnetic arrangement of neighboring spins.

ported by our multiplet calculation (cf. Fig. 6). However, the calculation resolves the contributions of different multiplets to the peak at 5.6 eV, and it gives the relative weight of the different CT bands.

The calculated spectrum (see Fig. 6) shows only one strong CT band at 5.6 eV in ε_2^c , while in ε_2^a another strong CT band is observed at 4.5 eV. The latter results from an excitation into the lowest d^5 final state with $S=5/2$ (${}^6A_{1g}$). The next d^5 states (${}^4A_{2g}$, 4E_g , and ${}^4B_{1g}$) are found 0.9–1.5 eV above the ${}^6A_{1g}$ multiplet (see Fig. 7). The calculation shows that the second lowest excitation actually corresponds roughly to a transfer from O $2p$ to $3d_{xy}$ [see the sketch of $d^5({}^4A_{2g})$ in Fig. 9(b)], but excitations to $d^5({}^6A_{1g})$ and $d^5({}^4A_{2g})$ are forbidden along c by the orbital selection rule, as discussed above in the strong crystal-field limit for the lowest CT absorption. Only the transitions to $d^5({}^4E_g)$ and $d^5({}^4B_{1g})$ are allowed in the c direction [see sketch of the d^5 states in Figs. 9(a) and 9(c)]. These constitute the peak at 5.6 eV.

Along a , the peak frequency is somewhat lower (5.5 eV), reflecting the excitation to the ${}^4A_{2g}$ final state and a small anisotropy of the CT energy. From the fit of the entire spectrum, we find $\Delta_a=4.51$ eV and $\Delta_c=4.13$ eV. This is reasonable because the in-plane O(1) site and the apical O(2) site are crystallographically different.^{22,29}

We emphasize that the assignment is unique. The lowest CT excitation (hopping from O $2p$ to $3d_{x^2-y^2}$) is the strongest one in $\sigma_1^a(\omega)=(\omega/4\pi)\varepsilon_2^a$. Interpreting the peak at 3.5 eV or even the 2 eV band as the lowest CT excitation does not yield sufficient weight around 4.5 eV in $\sigma_1^a(\omega)$. Moreover, the selection rules show unambiguously that the peak at 5.6 eV along c corresponds to excitations to the $d^5({}^4E_g)$ and $d^5({}^4B_{1g})$ multiplets, which are 1.2–1.5 eV above the lowest d^5 state. Thus, we conclude that the lowest CT energy is ≥ 4 eV.

The increase of spectral weight in $\sigma_1^a(\omega)$ with increasing temperature (see top panel of Fig. 3) can partially be attributed to the decrease of $\sim 0.5\%$ of the Mn-O(2) distance d_c from 20 to 300 K.²² With $t_{pd} \propto d_c^{-4}$ (Ref. 40) and $\sigma_1^a \propto d_c^2 t_{pd}^2 \propto d_c^{-6}$, the decrease of d_c can only account for a change in SW of $\sim 3\%$, in contrast to the observed gain of $\sim 10\%$, see Fig. 3. This may reflect a change in the occupation of the $3z^2-r^2$ orbitals, see Sec. V C.

B. Mott-Hubbard excitations

The observed value of σ_1^a of a few $100 (\Omega \text{ cm})^{-1}$ around 2 eV is typical for a Mott-Hubbard absorption band in

transition-metal oxides, e.g., in $RTiO_3$ or RVO_3 .^{2,16,41,42} The SW around 2 eV cannot be attributed to local dd excitations (crystal-field excitations), which are parity forbidden within a dipole approximation. A finite SW is obtained by the simultaneous excitation of a symmetry-breaking phonon, typically resulting in σ_1 of only a few $(\Omega \text{ cm})^{-1}$.^{43,44}

First, we discuss the spin selection rule. The ground state is a $d^4({}^5A_{1g})d^4({}^5A_{1g})$ state (see Fig. 7), i.e., $S=2$ on both sites. If the spins are parallel ($S_i^z=2$ on both sites $i=1,2$), only fully spin-polarized states with $S(d^3)=3/2$ and $S(d^5)=5/2$ can be reached by the transfer of one electron with $S=1/2$. For antiparallel spins ($|S_1^z|=2$, $S_2^z=-S_1^z$), we can reach final states with $S(d^3)=3/2$ and $S(d^5)=3/2$ or $5/2$ ($|S^z|=3/2$ in both cases).

We start the peak assignment again from the strong crystal-field limit. The highest occupied orbital $d_{3z^2-r^2}$ on one site has overlap to both $d_{x^2-y^2}$ and $d_{3z^2-r^2}$ on the other site. In contrast, hopping of an electron from xy , yz , or zx is only finite to the *same* type of orbital. In LaSrMnO_4 , this selection rule is strict because the O octahedra are neither tilted nor rotated. Thus, one expects only three different Mott-Hubbard peaks in the strong crystal-field limit: (i) the excitation from $3z^2-r^2$ to x^2-y^2 with a high-spin $S(d^5)=5/2$ in the final state (see Fig. 8), this transition has the lowest energy according to Hund's rule (as long as Δ_{eg} is not too large); (ii) the excitation from either $3z^2-r^2$ or xy or from the degenerate yz , zx orbitals to the *same* orbital on the other site [$S(d^5)=3/2$, see Fig. 9], these excitations have the same energy in the strong crystal-field limit because the orbital quantum number is preserved in the transition, and all the final states show the same spin quantum numbers; (iii) again an excitation from $3z^2-r^2$ to x^2-y^2 , but this time with $S(d^5)=3/2$.

The Coulomb interaction gives rise to configuration mixing³⁷ and lifts the degeneracy of the excitations collected in (ii). However, the overall features of the result of our multiplet calculation are reproduced rather well by the crude approximation of the strong crystal-field limit discussed above. As shown in Fig. 7, the lowest d^3 , d^4 , and d^5 states have ${}^4B_{1g}$, ${}^5A_{1g}$, and ${}^6A_{1g}$ symmetries, respectively. Thus, the lowest MH excitation is from the $d^4({}^5A_{1g})d^4({}^5A_{1g})$ ground state to a $d^3({}^4B_{1g})d^5({}^6A_{1g})$ final state (Fig. 8). This statement is valid over a wide range of parameters. This transition is assigned to the broad feature observed around 2 eV in $\sigma_1^a(\omega)$ (see Fig. 6). The width is attributed to the large bandwidth of the x^2-y^2 band. In the Drude-Lorentz fit described in the previous section, this excitation corresponds to peaks (1) and (2) [see Fig. 4(a)]. The fact that this feature is not well de-

scribed by a single Lorentzian can be attributed to band structure effects of the broad x^2-y^2 band. Note that a similar “fine structure” was observed for the very similar lowest optical excitation in LaMnO_3 .⁹ Due to the high-spin character of the d^5 final state, the spectral weight is largest for parallel alignment of neighboring spins (see sketch in Fig. 8). As discussed above, a d^5 final state with $S=5/2$ and $S^z=3/2$ is also possible for antiparallel spins in the antiferromagnetic state below $T_N=133$ K, but one expects a reduced SW. Figure 2 clearly shows an increase of the SW around 2 eV with increasing T , in agreement with our assignment.

Both the d^3 and the d^5 configurations show several multiplets that are less than ~ 1.5 eV above the lowest states. For the identification of the next higher-lying excitations, we thus have to consider the orbital selection rule. For the d^4 ground state, we find $\Gamma_{d^4}=A_{1g}$ (see Fig. 7), where Γ denotes an irreducible representation of the point group D_{4h} . The matrix elements $\langle d_i^5 | a_\tau^\dagger | d_k^4 \rangle \langle d_j^3 | a_{\tau'} | d_{k'}^4 \rangle$ are only finite for $\Gamma_{d^5} \otimes \Gamma_{a_\tau^\dagger} \supset A_{1g}$ and $\Gamma_{d^3} \otimes \Gamma_{a_{\tau'}} \supset A_{1g}$. For excitations with $\tau=\tau'$, i.e., hopping within the same type of orbital (see sketch in Fig. 9), we find $\Gamma_{d^5}=\Gamma_{d^3}$. According to Fig. 7 we can thus attribute the peak at 3.5 eV in $\sigma_1^a(\omega)$ to excitations with the final states $d^3(^4E_g)d^5(^4E_g)$, $d^3(^4A_{2g})d^5(^4A_{2g})$, and $d^3(^4B_{1g})d^5(^4B_{1g})$ [the higher-lying $d^3(^4E_g)d^5(^4E_g)$ transition has negligible weight], which roughly correspond to the hopping of an electron within the $d_{xz,yz}$, d_{xy} , and $d_{3z^2-r^2}$ orbitals, respectively. These excitations are degenerate within the strong crystal-field limit. According to the multiplet calculation, the splitting is only small, giving rise to one pronounced feature at 3.5 eV. Compared to the feature observed around 2 eV, the SW at low temperatures is larger at 3.5 eV because three different processes contribute and because of the spin selection rule. Since the final states have $S(d^5)=3/2$, the SW of these transitions is largest for the antiparallel alignment of neighboring spins. According to the Drude-Lorentz fit of the previous section, the feature at 3.5 eV indeed loses weight with increasing temperature [peak 3 in Fig. 4(b)]. The loss of $\sim 20\%$ from 15 to 330 K is not as strong as the gain of the lowest transition. The direct integration of $\sigma_1^a(\omega)$ from 2.8 to 4 eV even yields a slight gain of $\sim 3\%$ (see bottom panel of Fig. 3). As discussed above, this difference can be attributed to a change of the background which can be resolved by the Drude-Lorentz fit. However, a precise quantitative determination of the change of SW appears to be difficult in this frequency range, e.g., the background contribution of the CT transitions may have been underestimated in the Drude-Lorentz fit. The temperature dependence is discussed in more detail in the next section.

In comparison with the processes contributing to the peak at 3.5 eV, the excitation from $3z^2-r^2$ to x^2-y^2 with $S(d^5)=3/2$ is lower in Coulomb energy, but it costs about Δ_{eg} . This can be identified with the SW above ~ 4 eV in the MH contribution (see Fig. 6). Since $\tau \neq \tau'$, the orbital selection rule allows also for transitions to final states with $\Gamma_{d^5} \neq \Gamma_{d^3}$; thus, different multiplets contribute. However, these are difficult to separate from the CT excitations observed in the same energy range.

Our assignment is very well compatible with a number of different results. In LDA+ U calculations,^{25,45} the highest oc-

cupied band has mainly a Mn $3d_{3z^2-r^2}$ character (hybridized with O $2p$ bands) and the lowest unoccupied band is a Mn $3d_{x^2-y^2}$ band. Also, our interpretation of the peak at 3.5 eV is in agreement with the LDA+ U results.^{25,45} The x-ray data of Kuepper *et al.*²⁷ also suggest that the highest occupied states mainly have Mn character. Our results support the very similar interpretation of the lowest optical excitation in LaMnO_3 in terms of a Mott-Hubbard peak.^{5,6,9,46}

C. Temperature dependence and kinetic energy of the low-energy high-spin transition

The superexchange interaction between spins on neighboring Mn sites arises from the virtual hopping of electrons between the two sites. The intersite excitations probed in optical spectroscopy are the real-state counterpart of these virtual excitations. Therefore, the superexchange constant J is related to the spectral weight of the optical excitations.

In total, superexchange in LaSrMnO_4 favors antiparallel spins, but there is a ferromagnetic contribution J_{FM} , which corresponds to the lowest optical excitation to a high-spin $d^3(^4B_{1g})d^5(^6A_{1g})$ final state⁴⁷ [peaks (1) and (2) of the Drude-Lorentz fit, see Fig. 4(a)]. The relation between the spectral weight or N_{eff} of this excitation and J_{FM} has been derived^{18,48} for the d^4 compound LaMnO_3 . The c direction of LaMnO_3 with ferro-orbital order of $3x^2-r^2$ is equivalent to the a direction of LaSrMnO_4 with $3z^2-r^2$ orbitals. Adopting the formalism⁹ for LaSrMnO_4 , the effective carrier concentration N_{eff} , the in-plane kinetic energy K , and the ferromagnetic contribution to superexchange J_{FM} are related by

$$N_{\text{eff}} = \frac{m(2d_a)^2}{\hbar^2} K, \quad (3)$$

$$K = \frac{3}{8} J_{\text{FM}} \langle \vec{S}_i \vec{S}_j + 6 \rangle, \quad (4)$$

$$J_{\text{FM}} = \frac{t^2}{5E}, \quad (5)$$

where $2d_a=3.786$ Å is the Mn-Mn distance,²² m the free electron mass, i and j denote nearest-neighbor Mn sites, $t=(pd\sigma^a)/\Delta_a$ the effective Mn-Mn hopping amplitude, and $E=U_{\text{eff}}-3J_H+\Delta_{eg}$ denotes the excitation energy of the virtual intermediate state. We determined E from the weighted peak frequencies of peaks (1) and (2), $E=(N_{\text{eff}}^{(1)}E^{(1)}+N_{\text{eff}}^{(2)}E^{(2)})/N_{\text{eff}}=2.10$ eV at 15 K and 1.76 eV at 330 K. The nearest-neighbor spin-spin correlation is given by $\langle \vec{S}_i \vec{S}_j \rangle \rightarrow -4$ for $T \ll T_N$ and by $\langle \vec{S}_i \vec{S}_j \rangle \rightarrow 0$ for $T \gg T_N$. Using $\Delta_a=4.5$ eV from our analysis, we find $t=(pd\sigma^a)^2/\Delta_a \approx 0.6$ eV. Using $t=0.55-0.65$ eV, we derive $K(15 \text{ K})=\frac{3}{4}J_{\text{FM}}(15 \text{ K})=0.021-0.030$ eV and $K(330 \text{ K})=\frac{9}{4}J_{\text{FM}}(330 \text{ K})=0.077-0.108$ eV and finally $N_{\text{eff}}^{\text{AF}}(15 \text{ K})=0.040-0.056$ and $N_{\text{eff}}^{\text{para}}(330 \text{ K})=0.146-0.203$ [see Fig. 4(b)]. Both at low and at high temperatures, the calculated values agree amazingly well with the experimental results. This strongly corroborates our interpretation of the feature around 2 eV with the lowest Mott-Hubbard excitation.

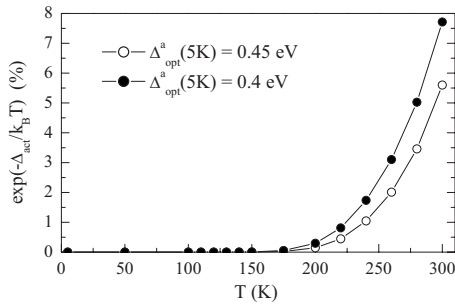


FIG. 10. Estimate of the thermally activated population of the UHB using $\Delta_{\text{act}}=(1/2)\Delta_{\text{opt}}^a$ and the temperature dependence of Δ_{opt}^a depicted in Fig. 5(b).

Moreover, it suggests that the redistribution of weight with temperature can be attributed mainly to a change of the nearest-neighbor spin-spin correlation function. As discussed above for the c direction, the change of the lattice constant may only account for a change of N_{eff} of a few percent.

A more detailed analysis requires the knowledge of the temperature dependence of $\langle \vec{S}_i \vec{S}_j \rangle$. In the three-dimensional antiferromagnet LaMnO_3 , the change of N_{eff} right at T_N is more pronounced.⁹ The more gradual changes observed in LaSrMnO_4 qualitatively agree with the expectations for a quasi-two-dimensional compound, in which $\langle \vec{S}_i \vec{S}_j \rangle$ is still significant above T_N .⁴⁹

D. Crystal-field excitations and thermal expansion

Up to 600 K, the c -axis lattice parameter shrinks with increasing temperature and the elongation of the octahedra is reduced. As a measure for the deviation from undistorted octahedra, we consider the difference between the apical Mn-O(2) and in-plane Mn-O(1) bond lengths, which amounts to $d_c - d_a \approx 0.39$ Å at 20 K and ≈ 0.37 Å at 300 K, i.e., it changes by more than 5%.²² The anisotropy of the thermal expansion has been interpreted as an indication for a change of the orbital occupation.²² The change of d_a across T_N may be rationalized in terms of the gain of magnetic energy with increasing J (induced by an increase in t), but the change of d_c suggests an orbital effect. On the basis of near-edge x-ray-absorption fine structure data, Merz *et al.* claimed a 15% occupation of x^2-y^2 orbitals at room temperature²⁸ as well as a transfer from x^2-y^2 to $3z^2-r^2$ with decreasing temperature.²⁹

Daghofer *et al.*^{30,31} studied the competition of various exchange contributions. For $\Delta_{eg}=0$, they find that x^2-y^2 is occupied on each site for the case of antiferromagnetic order. The fact that $3z^2-r^2$ is favored instead is due to $\Delta_{eg}>0$. Using $\Delta_{eg} \approx 0.1$ eV ~ 1160 K, Daghofer *et al.*³¹ find a significant redistribution of electrons from $3z^2-r^2$ to x^2-y^2 with increasing temperature. However, e_g electrons in general are strongly coupled to the lattice; thus, one expects much larger values, e.g., $\Delta_{eg} > 1$ eV in LaMnO_3 .⁴³ The transmittance is a very sensitive probe for low-lying crystal-field excitations,⁴³ but in LaSrMnO_4 , we do not find any evidence for crystal-field excitations below the optical gap (see Fig. 5). More-

over, our multiplet calculation yields $\Delta_{eg}=1.4$ eV (see Table I), in agreement with the strongly elongated O octahedra. More recently, Rosciszewski and Oles⁵⁰ pointed out that the $3z^2-r^2$ orbitals are occupied for $\Delta_{eg} > 0.1$ eV.

According to the Franck-Condon principle, optical excitations are very fast and probe the *static* crystal-field splitting, i.e., for a frozen lattice. For the thermal activation, one has to consider the minimal crystal-field splitting Δ_{eg}^{rel} after relaxation of the lattice. In optics, the peak frequency of a crystal-field absorption band corresponds to the static value Δ_{eg} (neglecting the phonon shift of 50–80 meV required for breaking the parity selection rule), whereas the onset of the absorption band can be identified with Δ_{eg}^{rel} . Our transmittance data for $T=5$ K clearly show that $\Delta_{eg}^{\text{rel}} > 0.4$ eV ~ 4600 K. Thus, we conclude that the thermal population of excited crystal-field levels, i.e., a *local* transfer of electrons from $3z^2-r^2$ to x^2-y^2 , is not sufficient to explain the anomalous thermal expansion.

The lowest electronic excitation corresponds to the optical gap $\Delta_{\text{opt}}^a \approx 0.4$ eV. The optical absorption process corresponds to the creation of *two* particles: an electron and a hole in a conventional semiconductor or an “empty” site (here d^3) and a “double occupancy” (here d^5) in a Mott-Hubbard insulator. With the Fermi energy lying in the middle of the gap, the thermal activation energy for a *single* particle is only $\Delta_{\text{act}}=(1/2)\Delta_{\text{opt}}^a \approx 0.2$ eV. In contrast, a crystal-field excitation corresponds to a *bound* electron-hole pair, i.e., an exciton, for which $\Delta_{\text{act}}=\Delta_{eg}$. As discussed above, the lowest Mott-Hubbard excitation with a $d^3(^4B_{1g})d^5(^6A_{1g})$ final state corresponds to the transfer of an electron from a $3z^2-r^2$ orbital to the x^2-y^2 band, similar to the local crystal-field excitations in the scenario proposed by Daghofer *et al.*^{30,31} However, the gain in kinetic energy of the *delocalized* d^5 final state is essential to obtain a small activation energy. A rough estimate of the thermally activated population of the x^2-y^2 UHB is obtained from $\exp(-\Delta_{\text{act}}/k_B T)$, using $\Delta_{\text{opt}}^a = 0.4-0.45$ eV at 5 K, the temperature dependence of Δ_{opt}^a depicted in Fig. 5(b) and $\Delta_{\text{act}}=(1/2)\Delta_{\text{opt}}^a$. The result is shown in Fig. 10. With a population of more than 5% at 300 K, the thermal activation into the UHB is a reasonable candidate for the explanation of the anomalous thermal expansion, at least above 150 K. Note, however, that the shrinkage of the c axis is already pronounced at lower temperatures.

Irrespective of the mechanism, we may ask to which extent our data support such a transfer. A change of the orbital occupation will slightly affect the orbital selection rule. One may speculate that the 10% *increase* of the SW of the CT excitations observed in the c direction (see top panel of Fig. 3) and the simultaneous 10% *decrease* of SW in $\sigma_1^a(\omega)$ above 4 eV partially are due to a reduced occupation of $3z^2-r^2$ and a slightly enhanced occupation of x^2-y^2 , respectively. This may explain the very similar T dependence of the c -axis lattice constant²² and N_{eff}^a above 4 eV. We emphasize that such a change of the orbital occupation of a few percent cannot explain the much more dramatic change of the SW of the lowest MH excitation around 2 eV.

Merz *et al.* reported a finite occupation of x^2-y^2 at 80 K.²⁹ This cannot be attributed to a thermal population but may reflect the important role played by hybridization. An-

other possibility for deviations from the regular orbital occupation is the disorder on the La/Sr sublattice. Each Mn ion has eight La/Sr neighbors, but due to La/Sr disorder, one may have to consider sites with a local surplus of Sr (or La) ions. In Sr_2MnO_4 , one finds d^3 Mn^{4+} ions. For a random La/Sr distribution, one expects that, e.g., about 1% of the Mn ions have seven or eight Sr neighbors. It is plausible that the d^4 configuration is not very stable at these sites, and one may speculate whether in this case x^2-y^2 is preferable over $3z^2-r^2$ so that the electron can spread out further to neighboring sites. Typically, one expects that more loosely bound electrons will give rise to absorption features below the optical gap. Lee *et al.*⁷ reported a peak at about 0.6 eV in LaSrMnO_4 at 10 K based on a Kramers-Kronig analysis of reflectivity data. They attributed this peak to impurities or O nonstoichiometry. Note that this peak at 0.6 eV has a maximum value of $\sigma_1(\omega) \approx 200$ ($\Omega \text{ cm}$)⁻¹, whereas the maximum of peak (1) at 1 eV is only about 60 ($\Omega \text{ cm}$)⁻¹ at 15 K [see inset of Fig. 2(b)]. This difference may point at a certain sample dependence of the data, supporting an interpretation in terms of impurities or disorder, but it may also reflect the problems of the Kramers-Kronig analysis. The room-temperature data of Moritomo *et al.*⁴ are in good agreement with our results. Above, we attributed both peaks (1) and (2) to the lowest MH excitation of the regular d^4 compound. The presence of two distinct peaks can be explained as a band structure effect. A very similar splitting has been observed⁹ in LaMnO_3 . We emphasize that the spectral weight of peak (1) is only small; its interpretation does not affect the assignment of all other peaks discussed above.

VI. CONCLUSION

Using a local multiplet calculation, we analyze $\sigma_1^a(\omega)$ and $\sigma_1^c(\omega)$ of LaSrMnO_4 from 0.75 to 5.8 eV. We arrive at a detailed peak assignment in terms of the multiplet splitting of charge-transfer and Mott-Hubbard excitations. We obtain an excellent description of the pronounced anisotropy and of the relative spectral weights of the different absorption bands. Applying the selection rules of an effective Mott-Hubbard model, the behavior of the lowest electronic excitations is described very well. In particular, the strong change of the spectral weight of the lowest excitation as a function of temperature can be attributed to the change of the nearest-neighbor spin-spin correlations $\langle \vec{S}_i \vec{S}_j \rangle$ in the Mott-Hubbard case. We thus conclude that LaSrMnO_4 can effectively be discussed as a Mott-Hubbard insulator. In this sense, the lowest optical excitation is from a $d^4(^5A_{1g})d^4(^5A_{1g})$ ground state to a $d^3(^4B_{1g})d^5(^6A_{1g})$ final state.

The clear advantage of the multiplet calculation over, e.g., a much simpler discussion of the strong crystal-field limit is that it yields a description of the entire spectrum as well as a full set of effective parameters. We find $U_{\text{eff}}=2.2$ eV and $J_H=0.6$ eV for the Coulomb interaction, $\Delta_a=4.5$ eV and $\Delta_c=4.1$ eV for the charge-transfer energy, and $10 Dq=1.2$ eV, $\Delta_{2g}=0.2$ eV, and $\Delta_{eg}=1.4$ eV for the crystal-field splitting of the d^4 configuration. The rather small value of U_{eff} is the result of our effective model, which does not consider hy-

bridization explicitly. Neglecting the hybridization most probably gives rise to the main shortcoming of our approach: it fails to describe quantitatively the anisotropy of the spectral weight, while the relative spectral weight of different peaks within $\sigma_1^a(\omega)$ is well described.

In transmittance measurements, we find $\Delta_{\text{opt}}^a=0.4-0.45$ eV at 15 K for the onset of excitations across the optical gap and 0.1–0.2 eV at 300 K. Due to this small value, the thermal population of the UHB may explain the anomalous shrinkage of the c -axis lattice parameter, at least above 150 K.

ACKNOWLEDGMENTS

We acknowledge the support by the DFG via SFB 608 and thank J. Baier for the specific heat measurements.

APPENDIX: OPTICAL-CONDUCTIVITY CALCULATION

In the considered frequency range (0.75–5.8 eV), $\sigma_1(\omega) = \sigma^{MH} + \sigma^{CT} + \sigma^{\text{hi}}$ shows MH and CT excitations as well as the onset of higher-lying bands such as $\text{La}(5d)$, $\text{Sr}(5s)$, $\text{Mn}(4s)$, and $\text{Mn}(4p)$.⁵ The latter correspond to the oscillator above the measured frequency range in the free fit (see Sec. III). The optical conductivity is calculated in arbitrary units by the Kubo formula.^{34,51–53} For layered LaSrMnO_4 , we assume $\sigma_1^{c,MH}=0$ because two Mn sites in different layers are far apart and the interlayer hopping is only small. The Mott-Hubbard contribution $\sigma_1^{a,MH}(\omega)$ reads

$$\sigma^{a,MH}(\omega) = \frac{4d_a^2}{N} \sum_{i,j,k,k'} \frac{\mathcal{M}_{i,j,k,k'}^{a,MH}}{E_{ij}^{MH}} \delta(\omega - E_{ij}^{MH}), \quad (\text{A1})$$

$$\begin{aligned} \mathcal{M}_{i,j,k,k'}^{a,MH} &= \left| \langle d_i^5 d_j^3 \sum_{\tau,\tau'} t_{\tau,\tau'}^{a,MH} a_{\tau}^{\dagger} a_{\tau'} | d_k^4 d_{k'}^4 \rangle \right|^2 \\ &= \left| \sum_{\tau,\tau'} t_{\tau,\tau'}^{a,MH} \langle d_i^5 | a_{\tau}^{\dagger} | d_k^4 \rangle \langle d_j^3 | a_{\tau'} | d_{k'}^4 \rangle \right|^2. \end{aligned} \quad (\text{A2})$$

Here, d_a denotes the in-plane Mn-O(1) bond length, $N=2$ the two different spin orientations in the antiferromagnetic ground state ($d_{\downarrow}^4 d_{\uparrow}^4, d_{\uparrow}^4 d_{\downarrow}^4$), and the indices i, j, k , and k' label the many-particle eigenfunctions, i.e., d_i^n refers to the i th eigenfunction of the d^n configuration with eigenenergy $E_i(d^n)$, $E_{i,j}^{MH} = E_i(d^5) + E_j(d^3) - 2E_0(d^4)$, a_{τ}^{\dagger} (a_{τ}) creates (annihilates) an electron in the orbital τ , where τ and τ' label the complex Mn $3d$ orbitals, and the dd hopping matrix $t_{\tau,\tau'}^{a,MH}$ indicates the overlap between two d orbitals via a bridging O ion. This matrix governs the orbital selection rules; it has been obtained from the Slater-Koster tabular.⁵⁴ The charge-transfer contribution $\sigma_1^{l,CT}(\omega)$ for $l=a$ or c has been calculated analogously.³³

For each excitation, the multiplet calculation gives the peak frequency ω_0 and the spectral weight, e.g.,

$$\omega_p^2/8 = \frac{4d_a^2}{N} \sum_{i,j,k,k'} \mathcal{M}_{i,j,k,k'}^{a,MH} / E_{ij}^{MH}. \quad (\text{A3})$$

For the line shape, we assume a Lorentz oscillator [see Eq. (2)]. The peak width γ cannot be derived from our local

model. As fit parameters, we employ γ^{CT} for all CT excitations and γ^{MH} for the MH peaks ($\gamma=2\gamma^{MH}$ for the peaks below 2.6 eV to account for the larger width of the x^2-y^2 band). For $T=15$ K, we find $\gamma^{CT}=1.10$ eV and $\gamma^{MH}=0.44$ eV. The onset of higher-lying bands is described by one oscillator with $\omega_0^{\text{hi}}=8$ eV, $\gamma^{\text{hi}}=2.8$ eV, and $\omega_p^{\text{hi}}=6.23$ eV at $T=15$ K, where only ω_p^{hi} has been varied in the fit. The contribution to ε_1 arising from all excitations lying at still higher energies is taken into account by $\varepsilon_{\infty}^a=1.37$ and $\varepsilon_{\infty}^c=1.51$. Since Eq. (6) is measured in arbitrary units, we use a global scaling factor A for $\sigma_1(\omega)$ (with $A=24.83$ from the

fit). The *anisotropy* of σ_1 is governed by the matrix elements. The hopping strength depends sensitively on the distance, $pd\sigma \propto d^{-4}$.⁴⁰ For Mn-O distances²² of $d_a=1.88$ Å and $d_c=2.28$ Å, one expects $pd\sigma^c/pd\sigma^a \approx 0.46$. Using this value, we underestimate the spectral weight of the single peak observed at 5.6 eV in $\sigma_1^c(\omega)$. Therefore, we scale $pd\sigma^c$ and $pd\pi^c$ with the common factor $A_c=1.96$. This failure of describing the anisotropy of the spectral weight quantitatively most probably reflects that we have neglected pd hybridization (see Ref. 33 for more details).

- 1 J. Zaanen, G. A. Sawatzky, and J. W. Allen, Phys. Rev. Lett. **55**, 418 (1985).
- 2 T. Arima, Y. Tokura, and J. B. Torrance, Phys. Rev. B **48**, 17006 (1993).
- 3 T. Mizokawa and A. Fujimori, Phys. Rev. B **54**, 5368 (1996).
- 4 Y. Moritomo, T. Arima, and Y. Tokura, J. Phys. Soc. Jpn. **11**, 4117 (1995).
- 5 J. H. Jung, K. H. Kim, D. J. Eom, T. W. Noh, E. J. Choi, J. Yu, Y. S. Kwon, and Y. Chung, Phys. Rev. B **55**, 15489 (1997).
- 6 M. A. Quijada, J. R. Simpson, L. Vasiliiu-Doloc, J. W. Lynn, H. D. Drew, Y. M. Mukovskii, and S. G. Karabashev, Phys. Rev. B **64**, 224426 (2001).
- 7 Y. S. Lee, T. Arima, S. Onoda, Y. Okimoto, Y. Tokunaga, R. Mathieu, X. Z. Yu, J. P. He, Y. Kaneko, Y. Matsui, N. Nagaosa, and Y. Tokura, Phys. Rev. B **75**, 144407 (2007).
- 8 K. Tobe, T. Kimura, Y. Okimoto, and Y. Tokura, Phys. Rev. B **64**, 184421 (2001).
- 9 N. N. Kovaleva, A. V. Boris, C. Bernhard, A. Kulakov, A. Pimenov, A. M. Balbashov, G. Khaliullin, and B. Keimer, Phys. Rev. Lett. **93**, 147204 (2004).
- 10 K. H. Ahn and A. J. Millis, Phys. Rev. B **61**, 13545 (2000).
- 11 J. S. Lee, M. W. Kim, and T. W. Noh, New J. Phys. **7**, 147 (2005).
- 12 J. S. Lee, Y. S. Lee, T. W. Noh, S.-J. Oh, J. Yu, S. Nakatsuji, H. Fukazawa, and Y. Maeno, Phys. Rev. Lett. **89**, 257402 (2002).
- 13 M. W. Kim, Y. S. Lee, T. W. Noh, J. Yu, and Y. Moritomo, Phys. Rev. Lett. **92**, 027202 (2004).
- 14 R. Rauer, M. Rübhausen, and K. Dörr, Phys. Rev. B **73**, 092402 (2006).
- 15 S. Miyasaka, Y. Okimoto, and Y. Tokura, J. Phys. Soc. Jpn. **71**, 2086 (2002).
- 16 A. A. Tsvetkov, F. P. Mena, P. H. M. van Loosdrecht, D. van der Marel, Y. Ren, A. A. Nugroho, A. A. Menovsky, I. S. Elfimov, and G. A. Sawatzky, Phys. Rev. B **69**, 075110 (2004).
- 17 G. Khaliullin, P. Horsch, and A. M. Oleś, Phys. Rev. B **70**, 195103 (2004).
- 18 A. M. Oleś, G. Khaliullin, P. Horsch, and L. F. Feiner, Phys. Rev. B **72**, 214431 (2005).
- 19 A. Gössling, R. Schmitz, H. Roth, M. W. Haverkort, T. Lorenz, J. A. Mydosh, E. Müller-Hartmann, and M. Grüninger, arXiv:cond-mat/0608531 (unpublished).
- 20 P. Reutler, O. Friedt, B. Büchner, M. Braden, and A. Revcolevschi, J. Cryst. Growth **249**, 222 (2003).
- 21 S. Larochelle, A. Mehta, L. Lu, P. K. Mang, O. P. Vajk, N. Kaneko, J. W. Lynn, L. Zhou, and M. Greven, Phys. Rev. B **71**, 024435 (2005).
- 22 D. Senff, P. Reutler, M. Braden, O. Friedt, D. Bruns, A. Cousson, F. Bourée, M. Merz, B. Büchner, and A. Revcolevschi, Phys. Rev. B **71**, 024425 (2005).
- 23 M. Kriener, Ph.D. thesis, University of Cologne, 2005.
- 24 W. B. Wu, D. J. Huang, G. Y. Guo, H. J. Lin, T. Y. Hou, C. F. Chang, C. T. Chen, A. Fujimori, T. Kimura, H. B. Huang, A. Tanaka, and T. Jo, J. Electron Spectrosc. Relat. Phenom. **137-140**, 641 (2004).
- 25 K. T. Park, J. Phys.: Condens. Matter **13**, 9231 (2001).
- 26 K. Kuepper, R. Klingeler, P. Reutler, B. Büchner, and M. Neumann, J. Appl. Phys. **99**, 08Q308 (2006).
- 27 K. Kuepper, R. Klingeler, P. Reutler, B. Büchner, and M. Neumann, Phys. Rev. B **74**, 115103 (2006).
- 28 M. Merz, P. Reutler, B. Büchner, D. Arena, J. Dvorak, Y. U. Idzerda, S. Tokumitsu, and S. Schuppler, Eur. Phys. J. B **51**, 315 (2006).
- 29 M. Merz, G. Roth, P. Reutler, B. Büchner, D. Arena, J. Dvorak, Y. U. Idzerda, S. Tokumitsu, and S. Schuppler, Phys. Rev. B **74**, 184414 (2006).
- 30 M. Daghofer, A. M. Oleś, D. R. Neuber, and W. von der Linden, Phys. Rev. B **73**, 104451 (2006).
- 31 M. Daghofer, D. R. Neuber, A. M. Oleś, and W. von der Linden, Phys. Status Solidi B **243**, 277 (2006).
- 32 R. M. A. Azzam and N. M. Bashara, *Ellipsometry and Polarized Light* (Elsevier, New York, 1987).
- 33 A. Gössling, Ph.D. thesis, University of Cologne, 2007; <http://nbn-resolving.de/urn:nbn:de:hbz:38-21379>
- 34 M. Dressel and G. Grüner, *Electrodynamics of Solids: Optical Properties of Electrons in Matter* (Cambridge University Press, Cambridge, 2002).
- 35 M. Cardona, Solid State Commun. **133**, 3 (2005).
- 36 M. Cardona and M. Thewalt, Rev. Mod. Phys. **77**, 1173 (2005).
- 37 S. Sugano, Y. Tanabe, and H. Kamimura, *Multiplets of Transition-Metal Ions in Crystals*, Pure and Applied Physics Vol. 33 (Academic, New York, 1970).
- 38 M. W. Haverkort, Ph.D. thesis, University of Cologne, 2005; <http://nbn-resolving.de/urn:nbn:de:hbz:38-14558>, arXiv:cond-mat/0505214.
- 39 Within the Kanamori scheme, $U_{\text{eff}} = F^0 + (4/49) F^2(d^4) + (36/441) F^4(d^4)$ and $J_H = (2.5/49) F^2(d^4) + (22.5/441) F^4(d^4)$. With $F_{HF}^2(d^4) = 11.42$ eV and $F_{HF}^4(d^4) = 7.42$ eV, this corresponds to $U_{\text{eff}} = F^0 + r \cdot 1.54$ eV and J_H

- $=r \cdot 0.96$ eV. In contrast, the simple scheme uses $U_{\text{simple}}=F^0=1.2$ eV and $J_{H,\text{simple}}=(1/14) [F^2(d^4)+F^4(d^4)]=r \cdot 1.41$ eV.
- ⁴⁰W. A. Harrison, *Elementary Electronic Structure* (World Scientific, Singapore, 1999).
- ⁴¹Y. Okimoto, T. Katsufuji, Y. Okada, T. Arima, and Y. Tokura, *Phys. Rev. B* **51**, 9581 (1995).
- ⁴²M. Imada, A. Fujimori, and Y. Tokura, *Rev. Mod. Phys.* **70**, 1039 (1998).
- ⁴³R. Rückamp, E. Benckiser, M. W. Haverkort, H. Roth, T. Lorenz, A. Freimuth, L. Jongen, A. Möller, G. Meyer, P. Reutler, B. Büchner, A. Revcolevschi, S.-W. Cheong, C. Sekar, G. Krabbes, and M. Grüninger, *New J. Phys.* **7**, 144 (2005).
- ⁴⁴C. J. Ballhausen, *Introduction to Ligand Field Theory* (McGraw-Hill, New York, 1962).
- ⁴⁵Hua Wu (unpublished).
- ⁴⁶S. Grenier, J. P. Hill, V. Kiryukhin, W. Ku, Y.-J. Kim, K. J. Thomas, S.-W. Cheong, Y. Tokura, Y. Tomioka, D. Casa, and T. Gog, *Phys. Rev. Lett.* **94**, 047203 (2005).
- ⁴⁷L. F. Feiner and A. M. Oleś, *Phys. Rev. B* **59**, 3295 (1999).
- ⁴⁸G. Khaliullin, *Prog. Theor. Phys. Suppl.* **160**, 155 (2005).
- ⁴⁹P. A. Fleury and H. J. Guggenheim, *Phys. Rev. Lett.* **24**, 1346 (1970).
- ⁵⁰K. Rościszewski and A. M. Oleś, *J. Phys.: Condens. Matter* **19**, 186223 (2007).
- ⁵¹E. Dagotto, *Nanoscale Phase Separation and Colossal Magnetoresistance* (Springer, New York, 2003).
- ⁵²M. Cuoco, P. Horsch, and F. Mack, *Phys. Rev. B* **60**, R8438 (1999).
- ⁵³D. van der Marel, *Strong Interactions in Low Dimensions*, Physics and Chemistry of Materials with Low-Dimensional Structures, Vol. 25 (Kluwer, Dordrecht, 2004), Chap. 8, p. 237.
- ⁵⁴J. C. Slater and G. F. Koster, *Phys. Rev.* **94**, 1498 (1954).